Detection of small cracks and cavities using laser diffraction

Xide Li
Tsinghua University
Department of Engineering Mechanics
Beijing, 100084, China
E-mail: huaf@mail.lib.tsinghua.edu.cn

A. K. Soh
University of Hong Kong
Department of Mechanical Engineering
Pokfulam Road
Hong Kong

Cong Huang
Tsinghua University
Department of Engineering Mechanics
Beijing, 100084, China

C. H. Yang
University of Hong Kong
Department of Mechanical Engineering
Pokfulam Road
Hong Kong

Hui-Ji Shi
Tsinghua University
Department of Engineering Mechanics
Beijing, 100084, China

Abstract. A good knowledge of the evolution process of a crack or cavity is necessary for a better understanding the mechanical behavior of the damage and failure of materials and structural components. Before damage begins, the size of the initial or prescribed cracks and cavities are usually very small. These small cracks and cavities can be conveniently used as the diffraction apertures of the coherent light. By analyzing the diffraction fields, the characteristic parameters of these special diffraction apertures can be obtained and, hence, the deformation fields. Experimental tests are conducted to demonstrate the reliability and accuracy of the laser diffraction technique in detecting the evolution and propagation of a small crack or cavity. The relationships between the coherent diffraction patterns and the crack and cavity geometric parameters are established for the simple shape of the crack or cavity aperture. Moreover, the autocorrelative method and the spectral iterative technique are introduced to retrieve the small crack and cavity apertures for the complex shapes.
[DOI: 10.1117/1.1474437]

Subject terms: laser diffraction; cracks and cavities; nondestructive testing; autocorrelation function; spectral restoration.

Paper 200331 received Aug. 18, 2000; revised manuscript received Sep. 18, 2001; accepted for publication Dec. 11, 2001.

1 Introduction

It is a known fact that the fatigue life of structural components consists of two discrete periods: the initiation of finite-sized cracks and subsequent propagation to failure. Consequently, it is important to develop a sensitive, nondestructive technique capable of detecting early fatigue damage *in situ*, to predict the remaining fatigue life of a component. Various optical techniques involving a laser light source have been used for nondestructive testing, which includes flaw detection and surface inspection. For example, the speckle correlation and speckle decorrelation techniques are used to inspect the surface fatigue deformation and surface morphology changes of the material.[1–4] A 1-D optical Fourier spectrum analysis system is applied to detect small fatigue cracks.[5] In addition, optical methods, such as photoelasticity, holography, moiré, speckle, and caustic are also widely used for crack detection or deformation measurement in a crack zone.[6–10]

Generally, all of the methods just mentioned have such advantages: sensitivity to the sample deformations (in plane or out of plane) and ability to make qualitative or quantitative full-field measurement of the displacements and displacement gradients (strains). But the disadvantages are also obvious, i.e., the requirement for a special test environment, such as vibration isolation, a dark room, and wet chemistry processing or special material and surface preprocessing. To properly evaluate the damage and failure of tested materials or structural components subjected to impact or cyclic loading, the inspection methods should be able to show instantaneous changes at the testing position, and keep track of cumulative degradation. This is a challenge to the scientists involved in experimental mechanics, which means that not only should the inspection system be as simple as possible, but the measurement method should also be adapted to *in situ* and original position testing.

In this paper, a relatively new optical technique, which is called the laser diffraction technique, was used to investigate the crack opening and propagation of a single slit crack and a cavity subjected to uniaxial tensile load. Moreover, this technique was also combined with the power spectrum autocorrelation method and spectral iterative technique, respectively, to retrieve the complex shapes of the microcrack and cavity apertures on the surface of the tested material.

2 Theory

2.1 *Basic Principles*

When the surface of a specimen that contains some small cracks and cavities is illuminated by a spatially filtered and collimated laser beam, the reflected and diffracted light intensity distributions carry the crack and cavity geometry information. Figure 1 shows a schematic diagram of the laser diffraction system. Before the diffracted pattern can

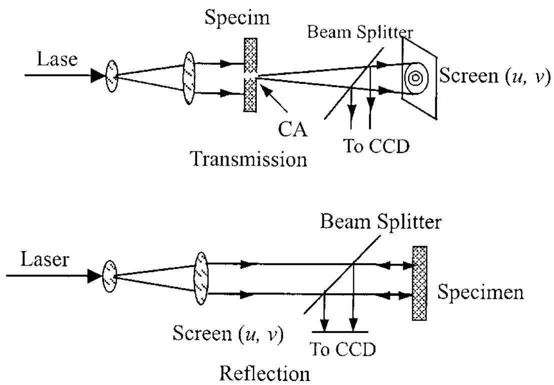

Fig. 1 Schematic diagram of the laser diffraction system for the evolution measurement of small cracks and cavities.

be applied for the study of the crack and cavity evolution, it is necessary to first discuss the relationship between the crack and cavity geometry and the intensity distribution diffracted from it. Obviously, when a small crack or cavity on the tested specimen is used as the diffracted aperture, the aperture shape is closely related to the crack or cavity geometry or the profile. The aperture formed by the small crack or cavity is called the crack or cavity aperture (CA), and it is mathematically described as the CA function $\Psi(x,y)$.

Suppose that the collimated laser illuminates the specimen uniformly in the normal direction and the light diffracted from the CA is observed on the receiving screen, as shown in Fig. 1. If the distance between the CA surface (x,y) and the observation plane (u,v) is so large that the Fraunhofer approximation can be used, the complex amplitude $A(u,v)$ at the (u,v)plane is given by[11]

$$A(u,v)=\frac{C}{j\lambda Z}\int_{-\infty}^{\infty}\int_{-\infty}^{\infty}\Psi(x,y)\times\exp\left[-j\frac{2\pi}{\lambda Z}(ux+vy)\right]\,\mathrm{d}x\;\mathrm{d}y \qquad (1)$$

where C is a complex factor and its amplitude is assumed to be one unit, and Z is the distance between the observation plane and the specimen surface. The integral of Eq. (1) is the Fourier transform of $\Psi(x,y)$ at the spatial frequencies. Since Eq. (1) is in the form of a 2D Fourier transform, the diffraction pattern can be expressed in Fourier transform notation as follows

$$A(f_x,f_y)=\frac{C}{j\lambda Z}\overline{\Psi}(f_x,f_y), \qquad (2)$$

where

$$\overline{\Psi}(f_x,f_y)=\int_{-\infty}^{\infty}\int_{-\infty}^{\infty}\Psi(x,y)\times\exp\left[-j2\pi(xf_x+yf_y)\right]\,\mathrm{d}x\;\mathrm{d}y, \qquad (3)$$

$$f_x=u/\lambda Z,\quad f_y=v/\lambda Z. \qquad (4)$$

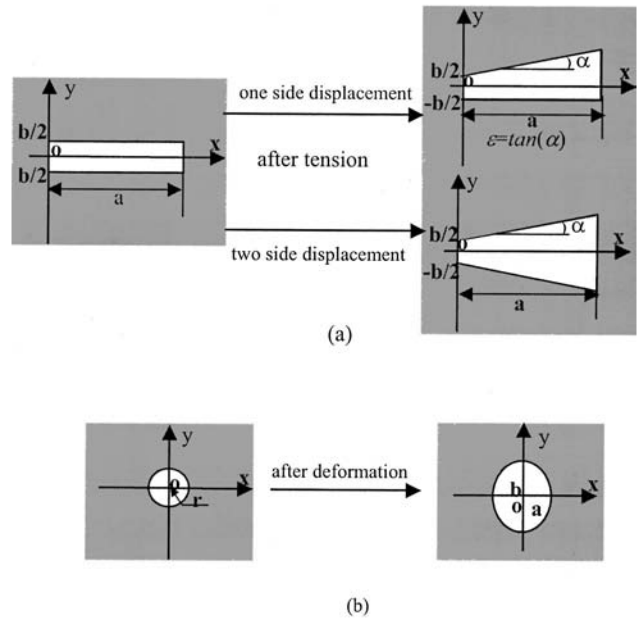

Fig. 2 Dimensions of the CA and the changes of shape caused by uniaxial tension: (a) a trapezoidal and (b) an elliptical CA.

The diffractive intensity recorded by the CCD camera on the (u,v) plane is

$$I(f_x,f_y)=\frac{1}{\lambda^2Z^2}\left|\int_{-\infty}^{\infty}\int_{-\infty}^{\infty}\Psi(x,y)\times\exp\left[-j2\pi(xf_x+yf_y)\right]\,\mathrm{d}x\;\mathrm{d}y\right|^2=\frac{1}{\lambda^2Z^2}|\overline{\Psi}(f_x,f_y)|^2. \qquad (5)$$

Equation (5) shows that the diffractive intensity is in proportion to the square of the spectrum of the crack aperture function $\Psi(x,y)$. Deformation or fatigue damage of the specimen changes the $\Psi(x,y)$ and hence alters its corresponding diffraction intensity. Thus, if the distribution of the diffraction intensity is measured, the change of $\Psi(x,y)$ can be evaluated.

2.2 *Analytical Reconstruction the Simple Geometry Shape of $\Psi(x,y)$ with Far-Field Laser Diffraction*

Two simple tensile specimens, one with a rectangular aperture and the other with a circular aperture were selected for a pilot study to simulate the simple geometry shape of a crack and a cavity. Their dimensions are given in Fig. 2. The corresponding intensity patterns of the diffraction fields can be expressed respectively as follows[11]:

$$I_r(f_x,f_y)=\frac{a^2b^2}{\lambda^2Z^2}\left|\sin c(af_x)\;\sin c(bf_y)\right|^2, \qquad (6)$$

$$I_c(r_f)=\left(\frac{D}{2\lambda Z}\right)^2\left|\frac{J_1(\pi D\rho)}{D\rho/2}\right|^2_{\rho=r_f/\lambda Z}, \tag{7}$$

where $J_1(x)$ is the first-order Bessel function of the first kind, $r_f=(f_x^2+f_y^2)^{1/2}$; and a, b, and D are crack length, width, and cavity diameter, respectively. Equations (6) and (7) produce 2D intensity distributions, where $I_r(f_x,f_y)$ is symmetric to both x and y axes, and $I_c(f_x,f_y)$ is circular symmetric. In the case of a rectangular CA, where $a>>b$, the main beam of the diffraction pattern of $I_r(f_x,f_y)$ is in the f_y direction. The values that make $I_r(f_x,f_y)$ and $I_c(f_x,f_y)$ zero are, respectively,

$$f_y=n/b,\quad n=0,\pm1,\pm2,\ldots,\quad \text{for } I_r(f_x,f_y), \tag{8}$$

$$\rho=\pm1.22/D,\ \pm2.23/D,\ \pm3.24/D,\ldots,\quad \text{for } I_c(\rho), \tag{9}$$

or

$$\Delta v=\frac{\lambda Z}{b}\quad \text{for } I_r(f_x,f_y), \tag{10}$$

$$\Delta r_f\approx1.01\lambda Z/D\quad \text{for } I_c(\rho), \tag{11}$$

where Δv and Δr_f are the distances between the n'th and $(n+1)$'th minimal along the f_y axis and the radial direction, respectively. Equations (8)–(11) show that the variables Δv and Δr_f or f_y and r_f, are inversely proportional to the width b and diameter D of the crack apertures, respectively. Therefore, both b and D can be determined by measuring the distances Δv and Δr_f. Thus, through the far-field diffraction of the laser beam, b and D can be measured with high accuracy.

The preceding $\Psi(x,y)$ functions are assumed for idealized rectangular and circular configurations. In the practical situation, the crack aperture varies in shape when the specimen is subjected to an applied load. Sections 2.3 and 2.4 deal with the complex apertures in the geometry shape. Assuming that the specimen is subjected to uniaxial tensile load and the deformation is small, the apertures of the rectangular and circular cavities will evolve and become approximately trapezoidal and elliptical, respectively, in shapes. Figure 2 shows the deformed aperture shapes. The diffraction fields due to trapezoidal and elliptical cavity apertures are be discussed in the following.

Figure 2(a) shows two kinds of trapezoidal cavity apertures, one consisting of a rectangle and a triangle and the other a rectangle and two triangles, which are due to one-side and two-side displacements, respectively, of the specimen during the uniaxial tensile test. By applying Eq. (3), the Fourier transforms of these two cavity apertures can be obtained as follows. For two-side displacement,

$$\begin{aligned}\overline{\Psi_{tt}(f_x},f_y)={}&ab\ \exp(-j\pi f_x a)\ \sin c(f_x a)\ \sin c(f_y b)\\&+\frac{ja}{2\pi f_y}\Big\{\exp(-j\pi b/2)\\&\times\exp[-j\pi(f_x+\varepsilon f_y)a]\ \sin c[(f_x+\varepsilon f_y)a]\\&-\exp\left(\frac{j\pi b}{2}\right)\ \exp[-j\pi(f_x-\varepsilon f_y)a]\\&\times\sin c(f_x+\varepsilon f_y)a+2j\\&\times\exp\\&(-j\pi f_x a)\ \sin(\pi f_y b)\ \sin c(f_x a)\Big\}.\end{aligned} \tag{12}$$

And for one-side displacement,

$$\begin{aligned}\overline{\Psi_{to}(f_x},f_y)={}&ab\ \exp(-j\pi f_x a)\ \sin c(f_x a)\ \sin c(f_y b)\\&+\frac{ja}{2\pi f_y}\ \exp(-j\pi f_x a)\ \exp(-j\pi f_y b)\\&\times\{\exp(-j\pi\varepsilon f_y a)\ \sin c[(f_x+\varepsilon f_y)a]\\&-\sin c(f_x a)\}.\end{aligned} \tag{13}$$

Equations (12) and (13) describe the far-field diffraction patterns of the trapezoidal apertures. These patterns are more complicated than those obtained from rectangular apertures. Note that the first terms on the right side of the equations are the far-field diffraction patterns of a rectangular aperture and the second terms are those of the triangular apertures. The parameter ε can be measured from the intensity distribution of the diffraction fields. In the present case, the limiting orientation of the diffraction is vertical to the crack surface. Thus the diffraction distribution along the $f_y=v/\lambda Z$ axis is considered. By inserting Eqs. (12) and (13) into Eq. (5), the intensity of the diffraction distributions can be expressed, for the first and second kinds of trapezoidal apertures, respectively, as follows:

$$I(f_{x0},f_y)=A(f_{x0},f_y)A^*(f_{x0},f_y)=\frac{1}{\lambda^2Z^2}\left|\overline{\Psi_{tt}(f_{x0}},f_y)\right|^2, \tag{14}$$

$$I(f_{x0},f_y)=A(f_{x0},f_y)A^*(f_{x0},f_y)=\frac{1}{\lambda^2Z^2}\left|\overline{\Psi_{t0}(f_{x0}},f_y)\right|^2, \tag{15}$$

where f_{x0} is a given frequency along the f_x axis. It is difficult to obtain the analytic solutions for the minimal values of $I(f_{x0},f_y)$. Therefore, the numerical solutions are presented in Fig. 3. By combining the numerical solutions with the distances between the n'th and $(n+1)$'th minimal of the diffraction intensities along the f_x and f_y axes obtained from the experiment, the changes of the geometric parameters of the CA can be measured for different loading states. Thus, such fracture parameters as the crack opening displacement, the stress intensity factor, and crack propagation can be obtained.

Similarly, for the elliptical crack aperture [refer to Fig. 2(b)], we have

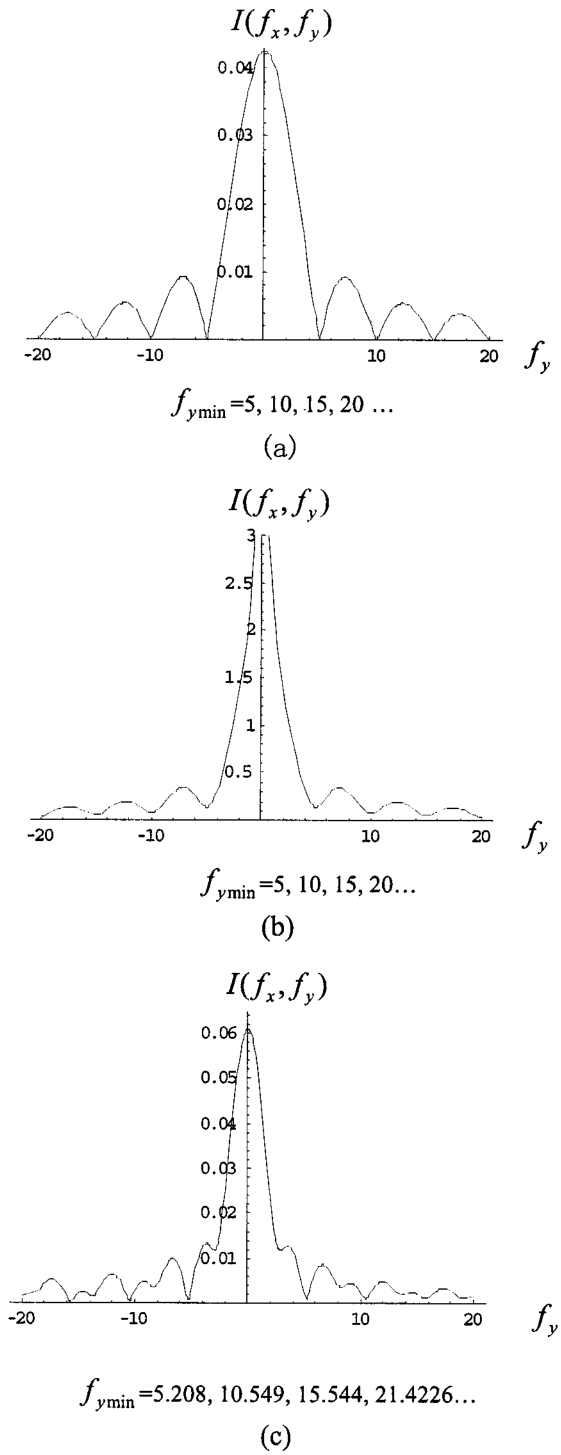

Fig. 3 Far-field diffraction patterns of rectangular/trapezoidal apertures: (a) $a = 5$ mm and $b = 0.2$ mm; (b) $a = 5$ mm, $b = 0.2$ mm, $f_x = 0.0$ and $\varepsilon=0.0349$; and (c) $a = 5$ mm, $b = 0.2$ mm, $f_x = 1.5$, and $\varepsilon = 0.0349$.

$$\overline{\Psi_e(f_x,f_y)} = \frac{2a}{\pi f_y} \sum_{n=-\infty}^{+\infty} \sum_{m=-\infty}^{+\infty} J_n(2\pi f_x a) J_{2m+1}(2\pi f_y b) \cdot P(n,m), \tag{16}$$

where $J_n(x)$ is the n'th order Bessel function of the first kind and $P(n,m)$ is defined as

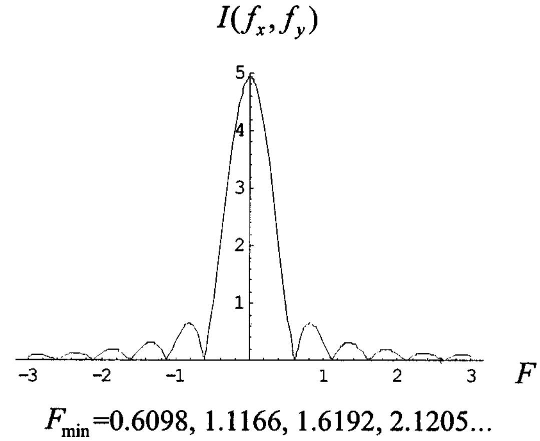

Fig. 4 Far-field diffraction pattern of a circular aperture, where $F = af_x$ is for the f_x axis and $F = bf_y$ is for the f_y axis.

$$P(n,m) = \begin{cases} \left.\begin{cases} 0 & m \neq \\ (-1)^n \pi/2 & m=0 \end{cases}\right\} n=0 \\ \left.\begin{array}{ll} \{[(n^2-4(m+1)^2]^{-1} - [n^2-4m^2]^{-1}\} n \sin n\pi/2 & n \in \text{odd} \\ \left.\begin{array}{ll} (-1)^m \pi/4 & n=2m \\ (-1)^m \pi/4 & n=2(m+1) \\ 0 & n \neq 2m \ \text{and} \ n=2(m+1) \end{array}\right\} n \in \text{even} \end{array}\right\} n \neq 0. \end{cases} \tag{17}$$

The intensity distribution of the elliptical crack aperture is

$$I(f_x,f_y) = A(f_x,f_y)A^*(f_x,f_y) = \frac{1}{\lambda^2 Z^2} \left| \overline{\Psi_e(f_x,f_y)} \right|^2. \tag{18}$$

The calculated results of Eq. (18) are presented in Fig. 4, and the values of $F_{\min}$ corresponding to the minimums of $I(f_x,f_y)$ are also listed in Fig. 4. Using these numerical results and Eq. (4), the changes of CA scale in different directions can be calculated.

2.3 *Spectral Autocorrelation Estimation of the Complex Geometry Shape of $\Psi(x,y)$ with Far-Field Laser Diffraction*

Equation (5) shows that the diffractive intensity is in proportion to the square of the spectrum of the aperture function $\Psi(x,y)$. Deformation or fatigue damage of the specimen causes the function $\Psi(x,y)$ to change and, hence, alters its corresponding diffraction intensity. If the distribution of the diffraction intensity is measured, the change of $\Psi(x,y)$ can be evaluated. However, when the shape of the cavity is complex, it is difficult to obtain the analytical diffraction formula from Eq. (5). Therefore, the evolution process of the complex aperture shape cannot be retrieved quantitatively. However, if the image of the crack or cavity is a bright and uniform distribution on the CA plane, the shape of the CA can be reconstructed by retrieving its support. First, we assume that the analysis is limited to Euclidean space of two dimensions, i.e., $(x,y) \in E^2$. Obviously, in the present case, $\Psi(x,y) \geqslant 0$ and the support S of $\Psi(x,y)$ is the smallest closed set such that the integral of

$\Psi(x,y)$ over the complement of S in E^2 is zero. Then the autocorrelation of $\Psi(x,y)$ can be defined as[12]

$$\rho_{\mathrm{CA}}(\zeta,\eta)=\int_{E^2}\Psi(x,y)^*\Psi(x+\zeta,y+\eta)\ \mathrm{d}x\ \mathrm{d}y$$
$$=\int_{E^2}\Psi(x,y)^*\Psi(x-\zeta,y-\eta)\ \mathrm{d}x\ \mathrm{d}y, \qquad (19)$$

where $\Psi(x,y)^*$ is the conjugate of $\Psi(x,y)$. If the support S of $\Psi(x,y)$ is compact (i.e., closed and bounded) and if $A$is the support of $\rho_{\mathrm{CA}}(\zeta,\eta)$, then

$$A=\bigcup_{(x,y)\in S}[S-(x,y)]=\{\zeta-x,\eta-y:(x,y)\in S\}. \qquad (20)$$

Equation (20) can be viewed as being formed by successively translating S . If we assume that S is a convex set, all convex symmetric sets A will have at least one solution[12]

$$S=\tfrac{1}{2}A=\{(\zeta/2,\eta/2):(\zeta,\eta)\in A\}. \qquad (21)$$

Equation (21) shows that the support of CA is just half that of its autocorrelation function. Therefore, if A is obtained, the support of the CA can be determined.

Applying Wiener-Khintchine theorem, we have the relationship between $\rho_{\mathrm{CA}}(\zeta,\eta)$ and its Fourier modulus of $\Psi(x,y)$:

$$\rho_{\mathrm{CA}}(\zeta,\eta)=\int_{-\infty}^{+\infty}\int_{-\infty}^{+\infty}\left|\overline{\Psi}(f_x,f_y)\right|^2$$
$$\times\exp[2\pi i(f_x\zeta+f_y\eta)]\ \mathrm{d}f_x\ \mathrm{d}f$$
$$=(Z\lambda)^2\int_{-\infty}^{+\infty}\int_{-\infty}^{+\infty}I(f_x,f_y)$$
$$\times\exp[2\pi i(f_x\zeta+f_y\eta)]\ \mathrm{d}f_x\ \mathrm{d}f_y. \qquad (22)$$

Equation (22) shows that the autocorrelation function of CA is the inverse Fourier transform of the squared Fourier modulus, and $\rho_{\mathrm{CA}}(\zeta,\eta)$ can be calculated by taking the inverse of Fourier transform of the diffractive patterns obtained from the laser diffraction measurements. Furthermore, the support A can also be determined from the retrieved $\rho_{\mathrm{CA}}(\zeta,\eta)$.

2.4 *Spectral Iterative Retrieval of the Complex Geometry Shape of $\Psi(x,y)$ with Far-Field Laser Diffraction*

Two mentioned methods have been used to retrieve the CA in the laser diffraction technique. Their advantage is that only simple calculations are required to determine the deformed apertures based on far-field diffraction intensity. But the disadvantage is that autocorrelation method does not always produce unique solution and the analytical method can only retrieve the deformed apertures in a simple shape.

To retrieve the complex geometry shape of $\Psi(x,y)$ effectively with far-field laser diffraction, an iterative method that utilizes the iterative Fourier transformation back and forth between the CA and its Fourier domains is employed to estimate the complex shape of the crack or cavity. From Eq. (5), $\overline{\Psi}(x,y)$ can be stated as

$$\overline{\Psi}(f_x,f_y)=|\overline{\Psi}(f_x,f_y)|\ \exp[j\Phi(f_x,f_y)]$$
$$=\int_{-\infty}^{\infty}\int_{-\infty}^{\infty}\Psi(x,y)$$
$$\times\exp[-j2\pi(xf_x+yf_y)]\ \mathrm{d}x\ \mathrm{d}y. \qquad (23)$$

Equation (23) means giving the modulus$|\overline{\Psi}(f_x,f_y)|$and some knowledge of $\Psi(x,y)$, then one can reconstruct $\Psi(x,y)$. An equivalent problem is to reconstruct the phase function of the Fourier transform $\Phi(f_x,f_y)$, since then simply performing an inverse Fourier transform generates $\Psi(x,y)$. In our case, the squared modulus (diffrective intensity) has been measured and the constraint of $\Psi(x,y)$ is real and nonnegative.

There are several particularly successful approaches to solving this retrieval problem: the error-reduction algorithm,[13] the input-output approach,[14] and related algorithms.[12,15,16] These algorithms involve iterative Fourier transformation back and forth between the object and Fourier domains and application of the measured data or known constrains in each domain. In our paper, a simple and general method, the error-reduction algorithm, also referred to as Gerchberg-Saxton algorithm, is employed to retrieve the aperture of the complex geometry shape.

The error-reduction algorithm was originally invented in connection with the problem of reconstructing phase from two intensity measurements. It consists of the following four steps: (1) Fourier transformation of an estimate object; (2) replacing the modulus of the resulting computed Fourier transform with the measured Fourier modulus to form an estimate of the Fourier transform; (3) inverse Fourier transformation of this estimate; (4) replacing the modulus of the resulting computed image with the known constraints in the object domain to form a new estimate of the object. In equations, for the k'th iteration, this is

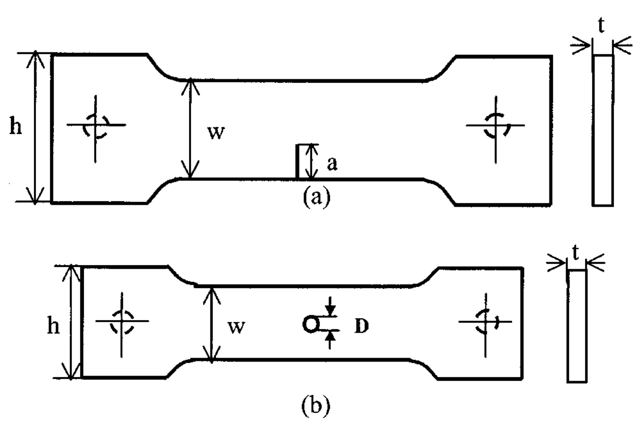

Fig. 5 Geometrical configurations of the specimens; (a) $h=20$ mm, $w=12$ mm, $a=5$ mm, and $t=2$ mm and (b) $D=0.5$ mm, $t=0.7$ mm, and $w=10$ mm.

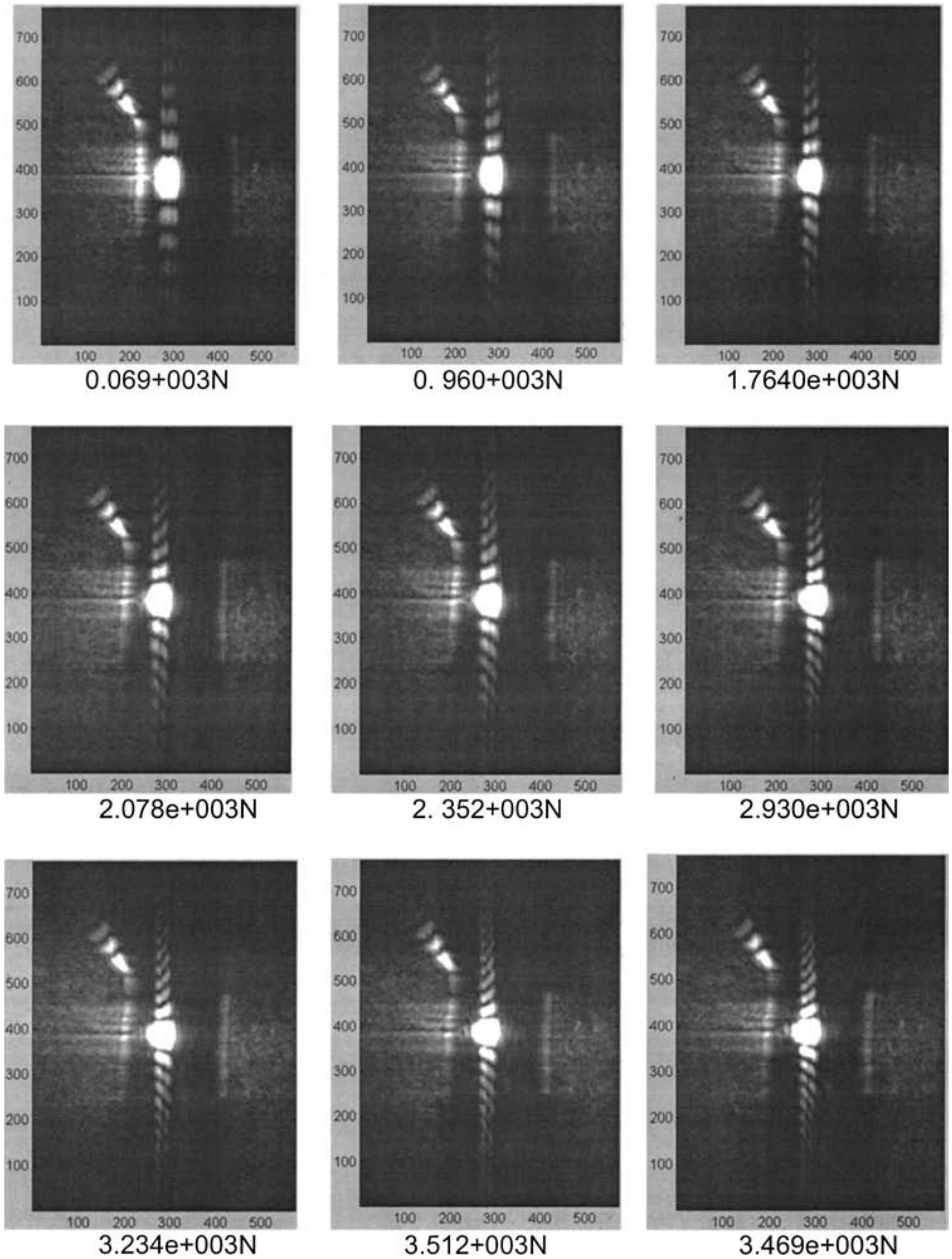

Fig. 6 Experimental results of the far-field diffraction patterns of an SEC aperture subjected to uniaxial tension.

$$G_k(f_x,f_y)=|G_k(f_x,f_y)|\exp[j\phi_k(f_x,f_y)]=\Im[g_k(x,y)], \tag{24}$$

$$G'_k(f_x,f_y)=|P(f_x,f_y)|\exp[j\phi_k(f_x,f_y)], \tag{25}$$

$$g'_k(x,y)=|g'_k(x,y)|\exp[j\theta_k(x,y)]=\Im^{-1}[G'_k(f_x,f_y)], \tag{26}$$

$$\begin{aligned} g_{k+1}(x,y)&=|g_{k+1}(x,y)|\exp[j\theta_{k+1}(x,y)] \\ &=|g_{k+1}(x,y)|\exp[j\theta_k(x,y)], \end{aligned} \tag{27}$$

where $g_k(x,y)$, $\theta_k(x,y)$, $G'_k(f_x,f_y)$, and $\phi_k(f_x,f_y)$ are estimates of $\Psi(x,y)$, $\varphi(x,y)$, $|\overline{\Psi}(f_x,f_y)|=I[(f_x,f_y)]^{1/2}$, and $\Phi(f_x,f_y)$, respectively. Here $\varphi(x,y)$ is the phase function of the input object. In our case, $\varphi(x,y)$ satisfies $\varphi(x,y)=0$.

For single-intensity measurement, as in our case, we use the following equation in Eq. (27):

$$g_{k+1}(x,y)=\begin{cases} g'_k(x,y), & (x,y)\notin\Lambda \\ 0, & (x,y)\in\Lambda \end{cases} \tag{28}$$

where Λ is the set of points at which $g'_k(x,y)$ violates the object-domain constraints, i.e., wherever $g'_k(x,y)$ is nega-

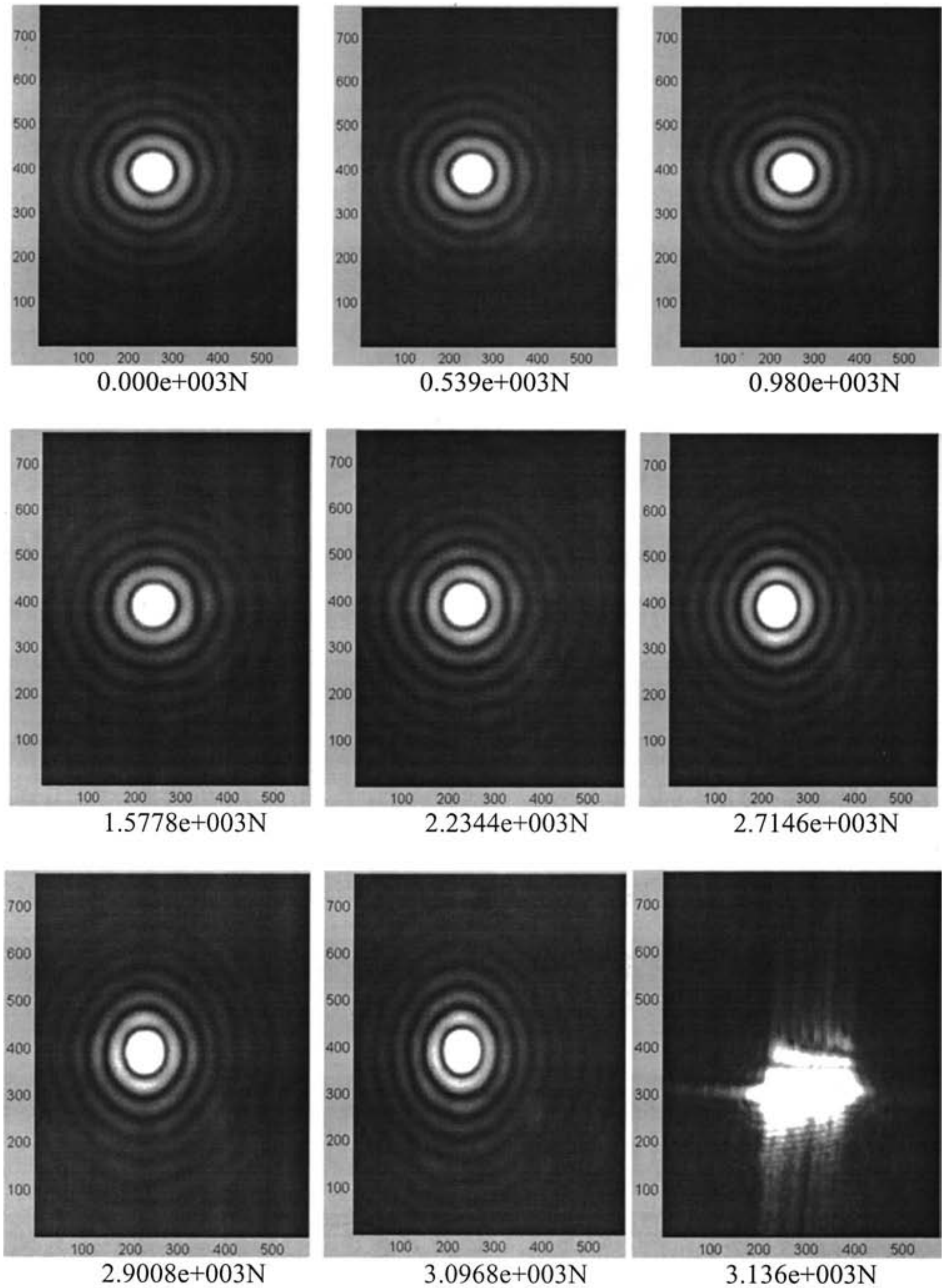

Fig. 7 Experimental results of the far-field diffractive patterns of a CCH aperture subjected to uniaxial tension.

tive or its dimension exceeds the know domain of the reconstructed object. The iterations continue until the computed Fourier transform satisfies the Fourier-domain constraints or the reconstructed image satisfies the object-domain constraints; then one has found a solution. The convergence of the algorithm can be monitored by computing the percent error, which can be expressed as

$$E_{frr}=\frac{\Sigma_{f_x,f_y}|[I(f_x,f_y)]^{1/2}-\mathrm{abs}(G_k(f_x,f_y)|}{\Sigma_{f_x,f_y}[I(f_x,f_y)]^{1/2}}\times 100\% \quad (29)$$

Equation (29) indicates when the squared error is zero, a solution has been found.

3 Experimental Procedure

3.1 *Uniaxial Tension Diffraction Experiments*

The uniaxial diffraction experiments were carried out to demonstrate the small crack and cavity evolution under loading. Figure 5 shows two specimens, one contains a single-edge crack (SEC) of length 5 mm and width 0.2 mm and the other contains a central circular hole (CCH) of radius 0.25 mm. The plate specimens are made of alumi-

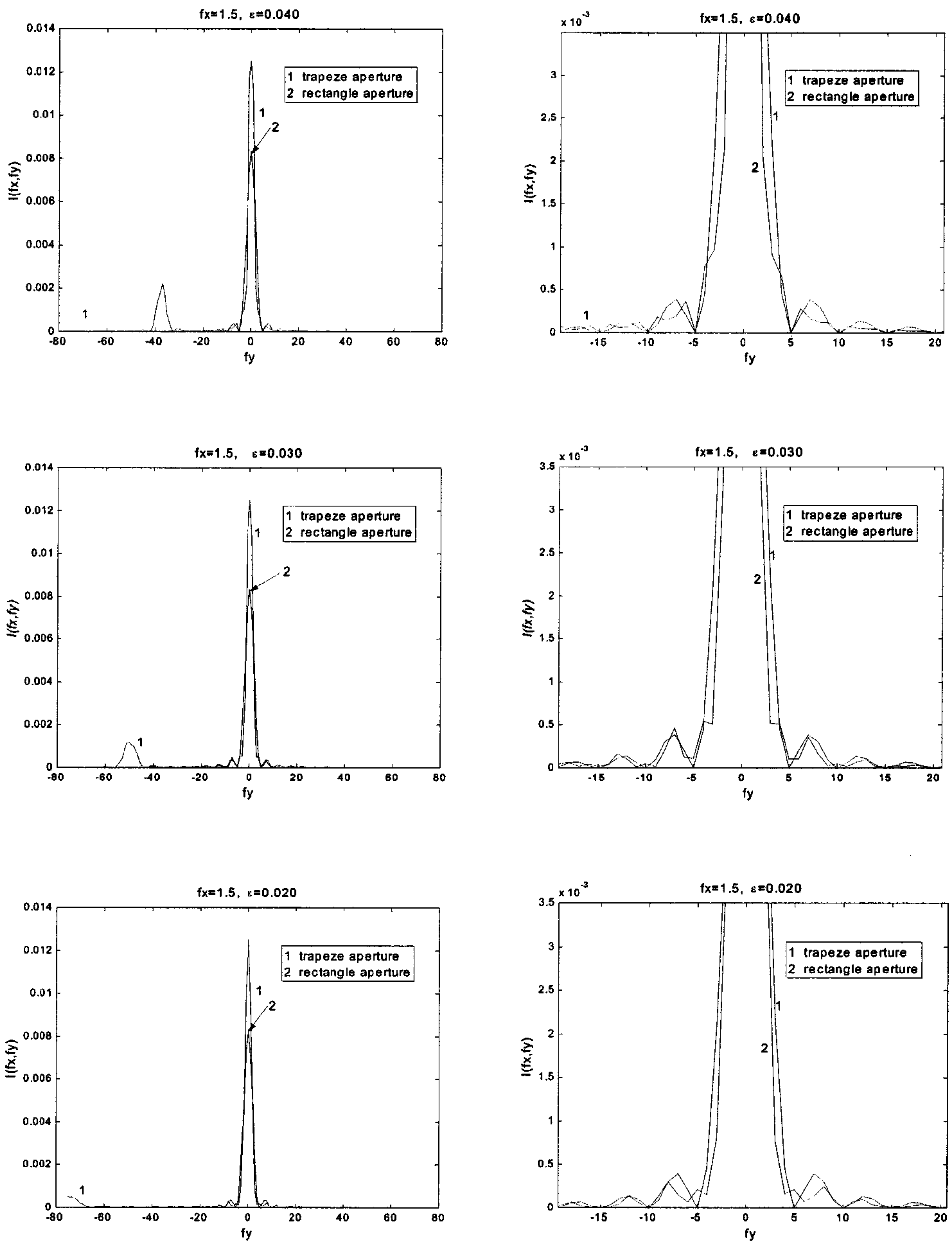

Fig. 8 Numerical calculations comparing the far-field diffraction patterns of the rectangular and trapezoidal apertures.

num alloy LY_{12} and manufactured using a wire-cut machine. The specimens were subjected to uniaxial tension, which produced one-side displacement. A digital force sensor recorded the applied loads. The specimen surface, consisting of an SEC or CCH, was illuminated by a collimated laser beam (refer to Fig. 1).

Figures 6 and 7 show the diffraction patterns of an SEC and a CCH at the observation plane. We found that the diffraction patterns contracted significantly with the increase of the loading. This phenomenon corresponded to the expansion of the CA when the specimens were subjected to tensile loading. The image system captured the diffraction pattern immediately and stored it into a personal computer. The distances between the n'th and $(n+1)$'th minimal of the diffraction pattern were detected automatically and the change of dimensions of the CA can be calculated by the formulas already given.

3.2 *Calculation of the Expansion of CA and Estimation of the Fracture Parameters*

Considering the actually loading state, we should use Eq. (15) to calculate the expansion δ of the crack surface for the SEC. However, it is clear to see that the distribution of the far-field diffraction patterns of the SEC is similar to the diffraction patterns of a slit with different widths. This means that the rotational component of δ was very small before rupture (brittle fracture), and thus Eq. (15) can be reduced to Eq. (6). To investigate the difference of the far-field diffraction patterns between the rectangular and trapezoidal apertures, both Eqs. (6) and (15) were used to cal-

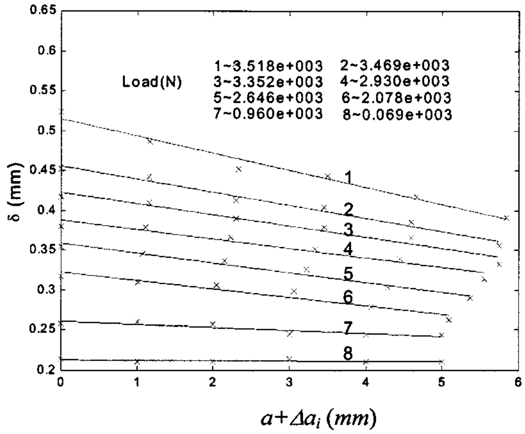

Fig. 9 Evolution curves of the SEC subjected to uniaxial tension.

culate the far-field diffraction patterns, by assuming that $a=5$ mm, $b=0.2$ mm, and ε was varied. Figure 8 presents the calculated results, which show that the strong subdiffraction (due to diffraction of a triangle) almost disappears at $\varepsilon=0.02$ and $f_x=1.5\ \mathrm{mm}^{-1}$, and the diffractive patterns caused by the rectangular and trapezoidal apertures are

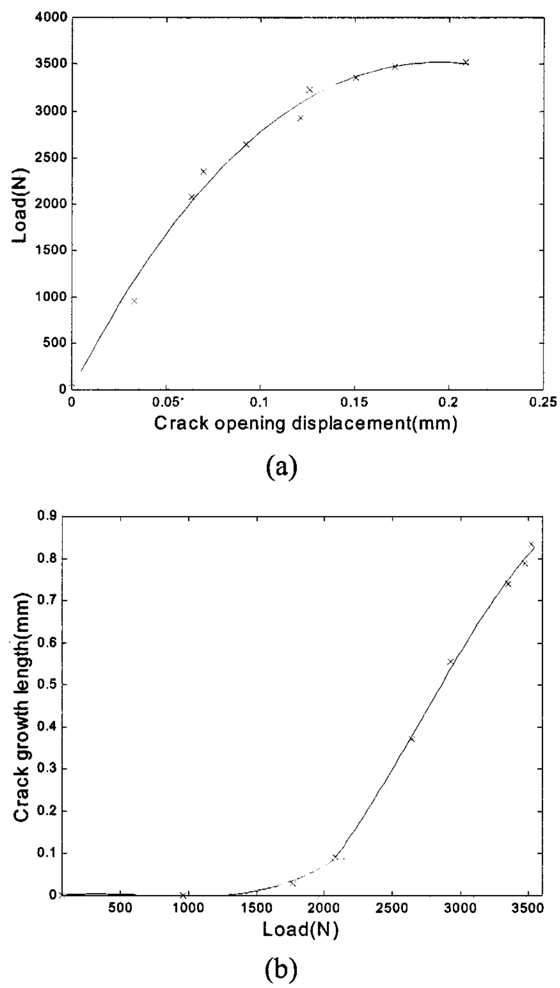

Fig. 10 Estimation of COD and Δa using evolution curves: (a) applied load versus COD and (b) Δa versus applied load.

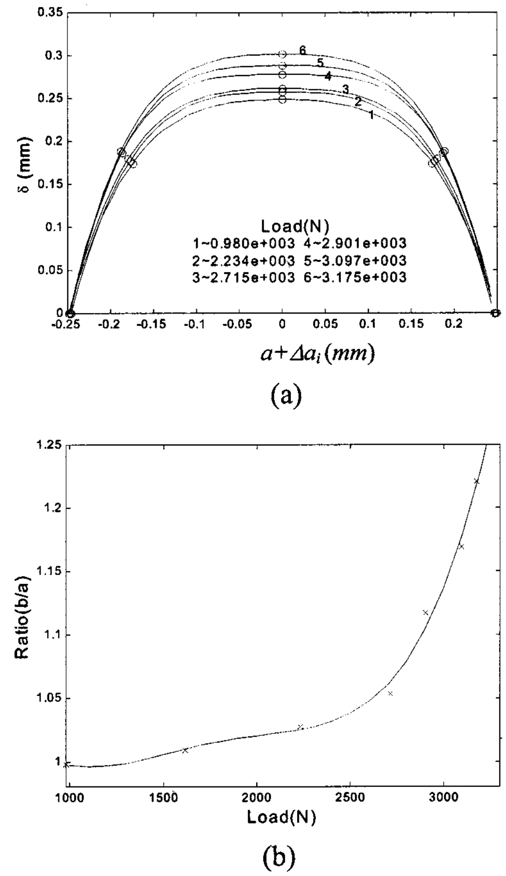

Fig. 11 Evolution curves (for plane $y\geqslant 0$) of the central circular cavity subjected to uniaxial tension: (a) expansion δ versus $a+\Delta a$ and (b) ratio of the major to minor axes versus applied load.

quite the same in the range of $f_y\in(-60,60)\ \mathrm{mm}^{-1}$. Thus, δ in the y axis (tensile direction) can be simply calculated using Eq. (6) when $\varepsilon<0.02$, which is deemed the condition of small angle opening of the CA. Figure 9 shows the evolution of δ at different stages of loading. The experimental data show that the evolution process can be divided into two parts: one is uniform expansion of the SEC, and the other is the rotation of the crack surface. The magnitudes of these two terms, which are estimated from curves 1 through 8 in Fig. 9, are 0.15 mm and 1.05 deg, respectively. Other important fracture parameters, such as crack opening displacement (COD), stress intensity factor (SIF), crack growth length (Δa), crack opening angle (COA), and crack tip opening angle (CTOA), can also be estimated from the evolution process of the SEC. Figure 10(a) shows the plot of applied load versus COD, and Fig. 10(b) presents the plot of Δa versus the applied load. The parameters of K_{IC}, CTOD, COA, and CTOA are estimated to be 20.30 MPam$^{1/2}$ ($\sigma^{\infty}=73.50$ MPa), 33.90 μm, 2.15 deg, and 20.98 deg, respectively. As for the case of CCH, Eq. (16) was used to calculate its expansion in the direction of 0, 45, 90, and 135 deg. Figure 11(a) shows the evolution process of the CA. The significant expansion can be clearly seen in the tensile direction. Figure 11(b) shows the ratio of the major to minor axes of the deformed elliptical CA during uniaxial tension. The maximum value of the expansion ratio is about 1.22 before rupture of the specimen occurs.

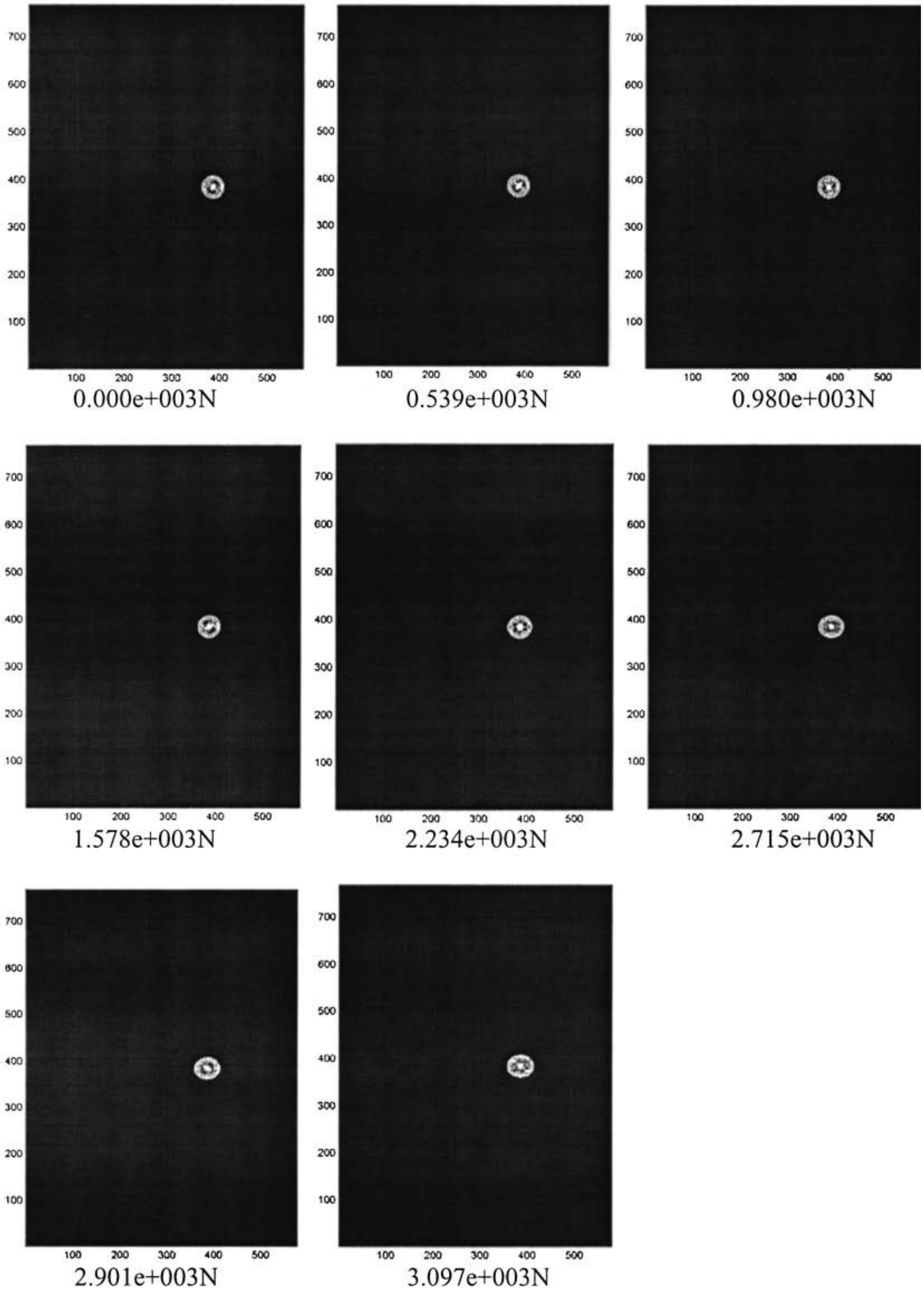

Fig. 12 Retrieval results of the deformed CA using autocorrelation function method, where loads are 3.0, 539.0, 980.0, 1577.8, 2234.4, 2714.6, 2900.8, and 3096.8 N, respectively.

3.3 *Cavity Aperture Estimation with Spectral Autocorrelation*

Based on the conclusion in Sec. 2.3, the support of a circle or an ellipse is just half that of its autocorrelation function. Therefore, the expansion δ of the CA can be easily retrieved from the autocorrelation function and the far-field diffraction intensity discussed in Sec. 2.2. Figure 12 shows the results of the retrieval for various applied loads. The evolution process of δ can be obtained from these retrieval images directly. The maximum ratio of the support in the tensile direction (horizontal direction) to that in the in-plane vertical direction was $58/47=1.23$ before rupture of the specimen occurred. This result tallied with the maximum ratio of the major to minor axes of the deformed CA when

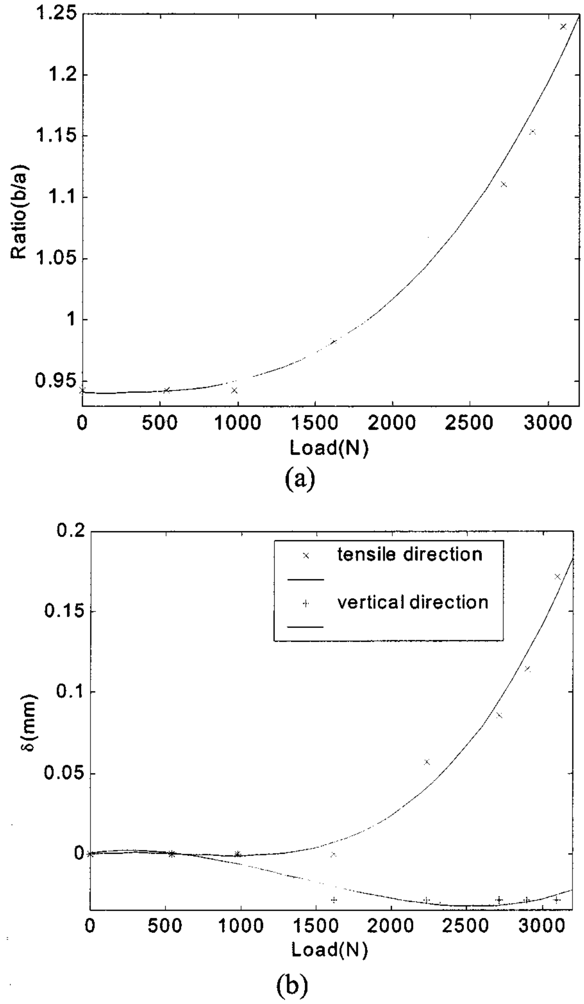

Fig. 13 Expansion of the deformed CA retrieved using the autocorrelation function; (a) the ratio of expansion in the horizontal direction (tensile direction) to that of vertical direction (free loading direction) versus applied load and (b) expansions of the deformed CA in the horizontal and vertical directions versus the applied load.

the specimen was subjected to uniaxial tension. Figure 13(a) presents the plot of the ratio *b/a* versus the applied load. The result indicates that the expansion in the tensile direction increased dramatically when the load exceeded 1000 N. Note that the initial ratio was not equal to 1, which indicates that the CA was not a circular cavity before the experiment was carried out. This was attributable to inaccurately drilling during the preparation of specimen. The tendency of rapid expansion maintained until the specimen ruptured. The amount of expansion δ is plotted against the applied tensile load in two directions, as shown in Fig. 13(b). The maximum expansions in the horizontal and vertical directions were 0.172 and -0.0285 mm, respectively. These results show that the necking effect was not obvious, which was expected because of the material property.

Another reconstructed specimen using the spectral autocorrelation method is a through microcavity on a silicon nitride lamella composite of aluminum matrix (thickness 1.3 mm). This material is widely used thanks to its super-high strength and light weight. However, when the material is applied with the flaky structure, the microcavities produced by pores in molten molding or by desquamating of the silicon nitride particles in machining will seriously effect the mechanical behaviors. Figure 14(a) shows the microscopic image of the cavity and Figs. 14(b) and 14(c) show the transmitted diffraction pattern and the reconstructed cavity aperture.

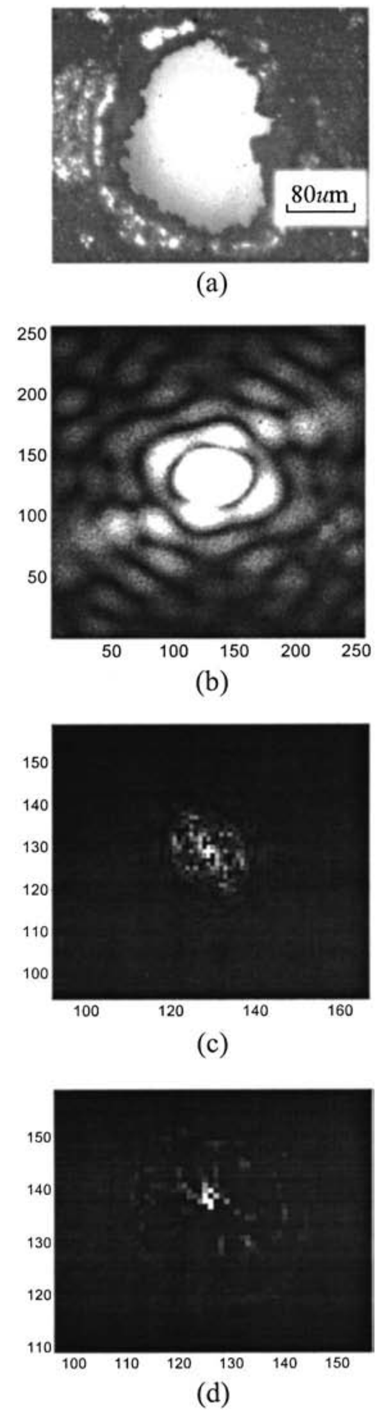

Fig. 14 Microcavity reconstruction: (a) the microscopic image of the cavity on the silicon nitride lamella composite of aluminum matrix, (b) far-field transmitted diffraction pattern of the through microcavity; (c) and (d) the reconstructed cavity with spectral autocorrelation method and spectral iterative method, respectively.

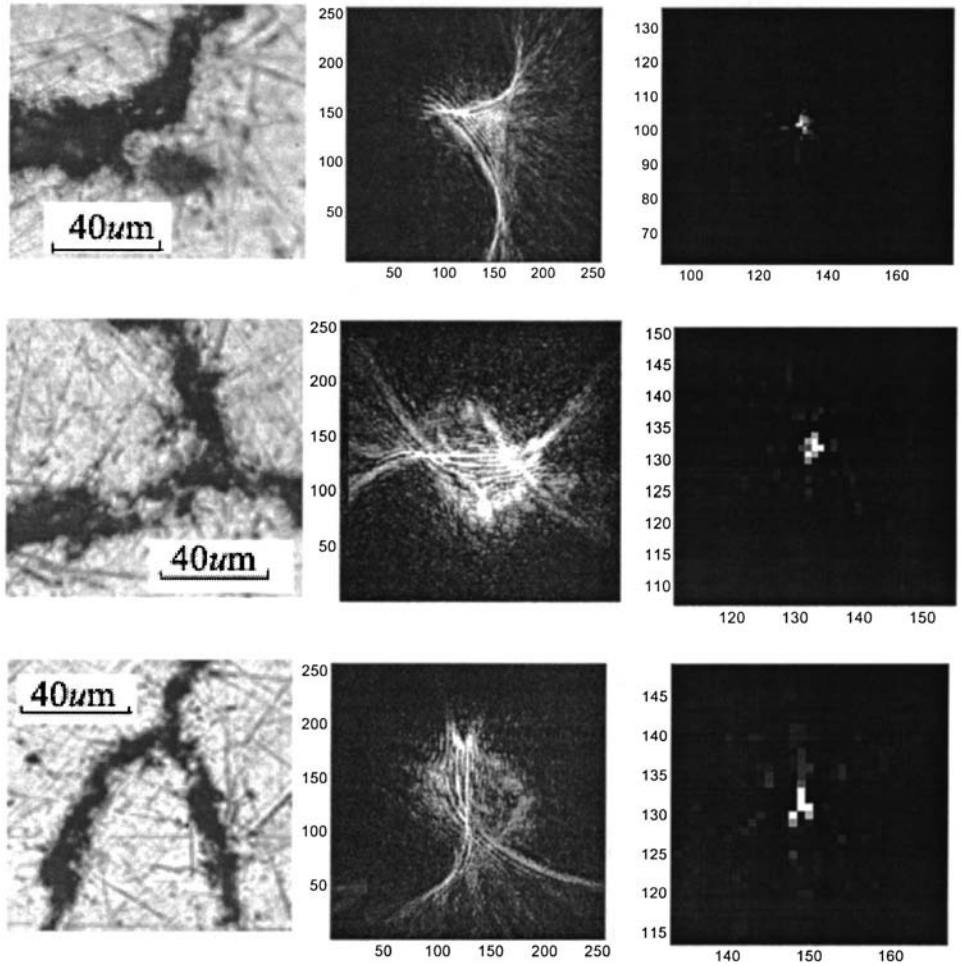

Fig. 15 Images of the microcracks on the surface of the ring and their corresponding far-field diffraction patterns and reconstructed microapertures: (from left to right: microcrack, diffraction pattern, and reconstructed microaperture).

3.4 *Micro CA Retrieval with the Spectral Iterative Method*

The spectral iterative method was used to reconstruct the microcrack on the surface of an aluminum alloy ring used in a bullet train. The reflected laser diffraction method is used to get the surface far-field diffraction patterns of the ring. It is well polished as a mirror surface before the experiment. The ring is subjected to diametral fatigue loading with a frequency of 106 Hz and compressed load amplitude 300 kg. After loading for 5 min, the reflected diffraction patterns corresponding to the different positions on the surface of the ring were recorded and reconstructed. Figure 15 shows the diffraction patterns and their corresponding reconstructed crack apertures. The microscopic images of the microcracks caused by the fatigue loading on the tested object are also shown in this figure (magnified 200 times). Finally, the microcavity aperture mentioned in Sec. 3.3 was also retrieved using the spectral iterative method. Figure 14(d) shows the retrieved result. The error in the spectral iterative method is limited by $E_{frr} \leqslant 6\%$.

4 Discussion

The laser diffraction technique was employed to investigate the evolution process of small cracks and cavities subjected to load. The experimental setup used is very simple but the interpretation of experimental data is relatively complicated. When the shape of the CA is simple, the aperture can be retrieved analytically from the far-field laser diffraction pattern. However, this is difficult in the case of a complex aperture. Therefore, any approach proposed is expected to provide qualitative or quantitative results about the evolution process of the complex aperture. The employment of autocorrelation function provides a simple calculation algorithm to retrieve the deformed CA. The significance of this method is twofold: (1) the ability to qualitatively estimate the cavity aperture *in situ* at the original position test and (2) the fact that it can be used as a limiting condition in the object domain for the spectral iterative method. The limitations are the convexity required for the CA shape and unique solution. Based on present knowledge, the supports of parallelograms, circles, ellipses, and convex polygons satisfy $S=A/2$. The supports of triangles can be retrieved by the posttreatment. Therefore, if the support of the CA is one of the convexities just listed, the CA can be retrieved from its autocorrelation function. The reconstructed images shown in Figs. 14(c) and 14(d) with the two retrieval methods have some differences, which are caused by the local nonconvex aperture of the cavity. The nonconvexity of the

CA extends the support of its autocorrelation function. Thus, the retrieval aperture size will be a bit larger than that of the real cavity.

The spectral iterative method is a convenient retrieval method that has no limitation on the geometry shape of CA. Attention is paid to the quality of the diffractive patterns, i.e., clear diffraction patterns should be received on the recording plane. This requires that the size of the CA should match the wavelength of the diffractive light, for example, 1 mm to several micrometers is a suitable aperture scale when a He-Ne laser is used as the coherent source. Another important point is to avoid the zero-order saturation and high-order loss of the diffractive intensity. This can be solved using a suitable aperture or a logarithmic look-up table while recording the diffraction patterns. Moreover, the cost on the iterative calculation is larger than that of the autocorrelation method. Meanwhile, the reconstructed aperture is small because of the microscale of the crack or cavity under test. Our future works will focus on promoting the calculated efficiency, enlarging the reconstructed CA (to accurately calculate the size of the micro-CA), and measuring the evolution of the complex geometry shape of the crack or cavity on site.

5 Conclusions

A methodology for estimating the evolution process of small cracks and cavities, using the laser diffraction technique, was investigated. The changes of the diffraction patterns during tensile testing of aluminum alloy specimens were observed; and several equations for expressing the relations between far-field laser diffractive patterns and small CA were derived. Two experimental tests were conducted to demonstrate the reliability and accuracy of the proposed technique for detecting the evolution process of a small crack or cavity with the simple in shape. The important fracture parameters, SIF, COD, COOD, COA, CTOA, and Δa are easily estimated using the evolution curves of the crack aperture versus the applied load, without measuring the whole field displacements of the specimen. Thus, the strict requirements for interferometry measurement, such as isolation of vibration, a complex optical setup, and a recording system are not necessary.

Two reconstruction algorithms, spectral autocorrelation and spectral iterative, were also employed together with the laser diffraction technique to estimate the small CA. The retrieved images and curves contain the evolution process of the deformed CA and structures of the microcrack or microcavity, respectively.

Acknowledgments

We gratefully acknowledge financial support by Project No. 10072031 supported by the NSFC, Special Funds for the Major State Basic Research Projects of China (No. G19990650), and the Research Grants Council of the Hong Kong Special Administrative Region, China (Project No. HKU 7081/00E).

References

1. Y. Z. Dai, A. Kato, and F. P. Chaing, ''Fatigue monitoring by laser speckle,'' *Int. J. Fatigue* **13**(3), 227–232 (1991).
2. J. S. Steckenrider and J. W. Wagner, ''Computed speckle decorrelation (CSD) for the study of fatigue damage,'' *Opt. Lasers Eng.* **22**, 3–15 (1995).
3. A. Kato and K. Tanabe, ''Non-contact strain measurement using metal foil gauges with the application of the laser speckle method,'' *Strain* **33**(1), 15–19 (1997).
4. A. Kato and M. Hayashi, ''Fatigue life estimation of steel using laser speckle senor,'' *NDT&E* **32**, 139–145 (1999).
5. B. J. Pernick and J. Kennedy, ''Optical method for fatigue crack detection,'' *Appl. Opt.* **19**(18), 3224–3228 (1980).
6. A. A. Wells and D. Post, ''The dynamic stress distribution surrounding a running crack—a photoelastic analysis,'' *Proc. SESA* **16**, 69–92 (1958).
7. D. Post, B.Han, and P. Ifju, *High Sensitivity Moiré: Experimental Analysis for Mechanics and Materials*, Springer-Verlag, New York (1994).
8. M. P. Boone, ''Use of reflection holograms in holographic interferometry and speckle correlation for measurement of surface displacement,'' *Opt. Acta* **22**(7), 579–589 (1975).
9. F. P. Chiang, ''A white light speckle method applied to the determination of stress intensity factor and displacement field around a crack tip,'' *Eng. Fract. Mech.* **15**(1–2), 115–121 (1981).
10. P. S. Theocaris, ''Elastic stress intensity factors evaluated by caustics in experimental evaluation of stress concentration and intensity factors,'' Chap. 3 in *Cracks in Composite Materials*, C. G. Sih, Ed., pp. 189–252, Martinus Nijhoff, The Netherlands (1981).
11. K. Iizuka, *Engineering Optics*, Springer-Verlag, Berlin (1985).
12. J.R. Fienup, ''Phase retrieval algorithms: a comparison,'' *Appl. Opt.* **21**(15), 2758–2214 (1982).
13. W. R. Gerchberg and W. O. Saxton, ''A practical algorithm for the determination of phase from image and diffraction plane pictures,'' *Optik (Stuttgart)* **35**, 237–246 (1972).
14. J. R. Fienup, ''Reconstruction of an object from the modulus of its Fourier transform,'' *Opt. Lett.* **3**(1), 27–29 (1978).
15. P.-T. Chen and M. A. Fiddy, ''Image reconstruction from power spectral data with use of point-zero locations,'' *J. Opt. Soc. Am. A* **11**(8), 2210–2214 (1994).
16. O. Hadar, E. Gersten, D. A. Weitzman, and D. Arbel, ''Image reconstruction from power spectral data,'' *Proc. SPIE* **2827**, 182–190 (1996).

Xide Li received his BS degree from the Department of Physics, Northwest University, in 1986 and his MS and PhD degrees in engineering mechanics in 1989 and in mechanical engineering in 1992, respectively, from Xi'an Jiaotong University. After completing his PhD degree, for 2 years he was a postdoctoral research fellow with the University of Science and Technology of China. From December 1996 to July 1997, he was a guest researcher at Lulea University of Technology in Sweden. He is currently an associate professor with Tsinghua University. His research fields are optical metrology and photomechanics. His research interests include the holographic interferometry, speckle interferometry, the digital correlation technique, phase-shifting measurement, computerized tomography, and computer digital image processing. He has been the leader responsible for several research projects and he has published about 40 papers in journals and proceedings.

A. K. Soh obtained his first degree from the University of Singapore and his PhD from the University of Surrey, United Kingdom. For several years he was a structural engineer with major onshore, marine, and offshore engineering firms prior to joining the Nanyang Technological University (NTU) as an academic staff member in 1983. He left NTU and joined the Department of Mechanical Engineering of the University of Hong Kong in 1996. His research interests include fracture study of piezoelectric and ferroelectric materials with defects and thin films, fatigue fracture analysis of tubular connections, and the development of new bimaterial finite elements.

Cong Huang received his BS from the Department of Engineering Mechanics of Tsinghua University in 2000. He is currently a master's student with the Institute of Mechanics, Chinese Academic School. His research interest is dynamic behaviors of materials.

C. H. Yang is a PhD candidate with the Department of Mechanical Engineering, the University of Hong Kong. His research interest is the analysis of finite elements.

Hui-Ji Shi holds a PhD and is a professor with the Department of Engineering Mechanics, Tsinghua University, where he directs the Central Laboratory of Materials Strength and Structural Vibration. His research is in solid mechanics concerning the fatigue and fracture of materials under severe environment conditions such as high-temperature and serious corrosion.